Romanian Reports in Physics, Vol. 67, No. 3, P. 1018–1027, 2015

HIGHLY ACCELERATED MICROPARTICLES IN PLASMA FLOWS

C.M. TICOŞ

National Institute for Laser, Plasma and Radiation Physics
Atomistilor 309, RO-077125, POB-MG36, Măgurele-Bucharest, Romania, EU
Email: catalin.ticos@inflpr.ro

Received December 5, 2013

Abstract. Rapid dust acceleration of dust grains of a few hundred microns in size was observed in laboratory plasma flows with density $\simeq 10^{19}$ m^{-3} and temperature of $\simeq 10$ eV. Specific issues related to dust material, detection and determination of the dust size, speed and acceleration are discussed. The measured dust acceleration is in agreement with predictions given by a plasma flow drag model.

Key words: plasma flow, dust, ion drag.

1. INTRODUCTION

Dust is ubiquitous in astrophysical, solar, and laboratory plasmas [1]. The motion of electrically charged micron size dusts in plasmas is determined by multiple forces simultaneously. These forces include gravity, electric force, plasma-flow drag force, neutral particles drag (in weakly ionized plasmas), and radiation pressure [2]. The magnitude of these different forces will vary under different plasma and dust conditions. In low ionized dusty plasmas with Debye length much larger than individual dust size, the first two forces are usually dominant [1, 3–8]. In flowing plasmas with Debye length smaller than the dust size, the plasma drag force is orders of magnitude higher than the other forces and can produce very large dust accelerations [9, 10].

Here, we report on the observation of plasma flow-dragged dust motion in laboratory dense plasmas flows with 3-D structure. The flow was produced in a coaxial plasma gun. The plasma was ejected along the gun axis and rotated about it. Although the flow seemed uniform, we show an instance were its direction varied at a scale of the order of a few millimeters, which produced dust traces with different orientation angles.

2. EXPERIMENT

The experiments were carried out on a large coaxial plasma gun as shown in Fig. 1 having the center electrode extended into the main vacuum chamber for $\sim$1.3

m to form a $\mathbf{E}_r \times \mathbf{B}_z$ configuration ('plasma annulus') to drive an azimuthal plasma rotation in the x-y plane.

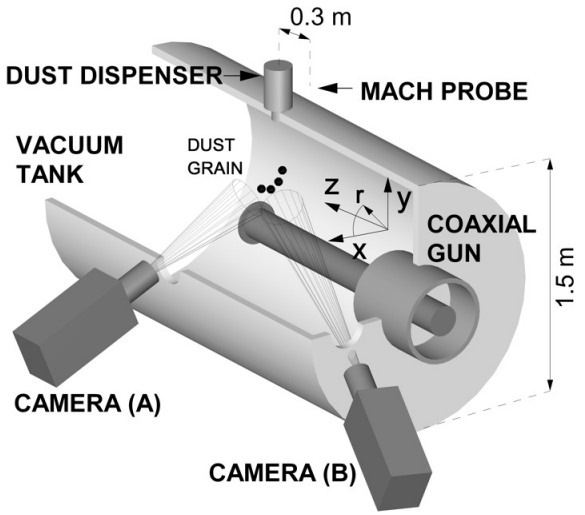

Fig. 1 – Coaxial plasma gun, dust dropper and high speed cameras, not to scale.

An electrolytic capacitor bank stored up to 300 kJ of energy at 900 V applied between the electrodes. An external axial magnetic field of 0.01 T was applied for all experimental data presented. The plasma diagnostics included Langmuir probes for measuring electron temperature, magnetic probes, a Mach probe for inferring the plasma flow speed, and two fast imaging cameras [11]. Helium gas was introduced from a puff-gas valve for a few ms. The pressure increased from a base 10^{-6} torr to a few mtorr when the shot was fired. Typical electron temperature was 3 - 15 eV, and plasma density was 0.5 - 5 $\times$ 10^{19} m^{-3}. Ion temperature (T_i) was inferred from spectroscopy line width measurements from the He II 468.57 nm line in a multichord ion Doppler spectrometer. We could conclude that ions were as hot as the electrons. The spectral line profile was fitted with a Gaussian profile, except at the wings [11].

2.1. DUST MATERIAL

A commercial powder which was essentially a special type of ink made of an aromatic heterocycle has been chosen for the experiment. The average size of the powder grains was smaller than 5 μm, as given by the manufacturer [12]. The grains were fluorescent and emitted light in the visible spectrum when illuminated by the UV plasma radiation. The powder looked white in daylight but changed color to yellow-green when shined with UV light. In our case optical excitation of the dust

material was realized by the He I 388.8 nm line of the plasma emission spectrum. Among other physical properties of the particles the mass-density of the microparticles was in the range 0.07 to 0.15 g/cm^3. The dust particles had a high adherence to each other. It seemed possible to release in the plasma only clusters of many dust particles. While this undesirable aspect lead to uncertainties concerning the size of the monitored dust particles, it was however helpful for the detection optics which had limited magnification when providing images of microscopic objects situated at roughly 1 meter from the camera, as is the case with camera (B).

The dust particles were stored in a dust reservoir on the top of the vacuum tank and were dispensed by vibrating an ultrasonic shaker [13]. The power of dust shaker and the size of the dust reservoir hole were both adjustable so that dust number density was low and dust-dust interaction could be neglected. The dust shaker was timed so that the dust particles, free falling due to gravity, were within both camera views at the start of a discharge. Dust fluorescence and the corresponding three-dimensional (3-D) dust trajectories were captured using two fast CCD cameras with roughly perpendicular views, one with a side view, and the other along the z-axis.

2.2. DUST PARTICLES DETECTION OF TRAJECTORIES

Direct detection and imaging of dust particles can be a challenging task. Its degree of difficulty depends on the size of the particles, the speed of the particles and the luminous flux scattered by them. In most dusty plasma cases the particles are static or slowly moving (a few mm/s) and are illuminated with a circular laser beam or a planar laser sheet. As the detection distance increases, powerful lenses are required with focal distance in the range 200 to 500 mm. The magnification is realized at the expense of lower light flux which results in images with a lower signal to noise ratio and with decreased contrast. The detection becomes even more complicated when the particles move rapidly within the field of view.

In our setup both camera were equipped with telescopic lenses with $f = 500$ mm. Camera 'A' recorded dust trajectory projection onto the y-z plane. The view 'B' corresponds to dust trajectory projection onto the x-z plane. Since the line-of-sight for the camera 'A' was not exactly in the x-direction (z-direction for camera 'B'), the corrected trajectories took into account line-of-sight information for both views. The resolutions of the two cameras were found to be 5.4 $\pm$ 0.1 pixel/mm for camera 'A' and 7.1 $\pm$ 0.1 pixel/mm for camera 'B'.

In order to measure the velocities and accelerations of the dust particles, we operated the cameras in the so-called 'multiple-trigger' mode. Each trigger led to a short exposure on the CCD detector that lasted between 10 to 40 μs, and trigger-to-trigger delay lasted 200 to 400 μs long, for a camera. Both cameras were triggered simultaneously by a pulse delay generator which was programmed in correlation with

the time $t = 0$ of the plasma shot. Up to five triggers applied for each image. This explains the four to five 'pearl'-like dots in each image of Fig. 2, with the 'center' of each dot corresponding to the instantaneous position of the dust. The dust particles locate between 0.4 to 0.6 m in radius. In terms of directions of dust motion, four types of dust trajectories have been identified using the two fast CCD cameras. In each case from (1) to (4), the view 'a' is recorded by the camera 'A', and the view 'b' is recorded by the camera 'B'.

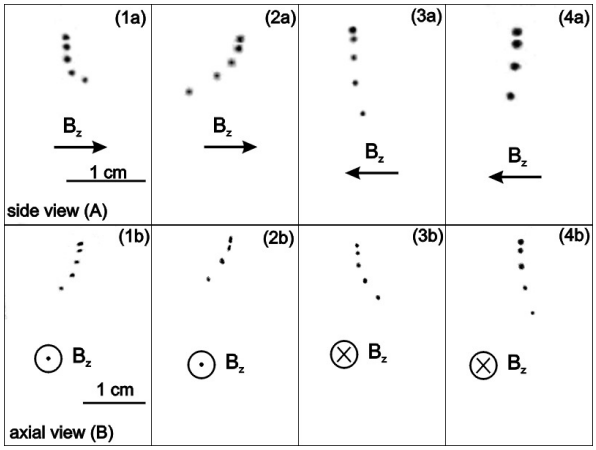

Fig. 2 – Each color inverted image shows a single dust particle captured in 4 or 5 frames: (a) are side images and (b) are axial images.

The cases (1) and (2) correspond to an external magnetic field pointing towards the plasma gun (negative z-direction), and the cases (3) and (4) are for an external magnetic field pointing away from the plasma gun (positive z-direction). Since an externally applied radial electric field always points to the center axis, $\mathbf{E}_r \times \mathbf{B}_z$ for cases (1) and (2) are counter-clock-wise in the azimuthal direction, and clock-wise for (3) and (4). The azimuthal rotations of the plasma were confirmed by Mach probe measurement [14]. Indeed, we also observed that (1b) and (2b) are in the counter-clock-wise direction, and (3b) and (4b) are in the clock-wise direction. For the same external $\mathbf{B}_z$, we observed the change in dust directions between (1a) and (2a), and between (3a) and (4a). These changes were due to the change of z-direction flows, as confirmed by the nine-electrode probe measurement [14]. One key observation is that the directions of dust trajectories are determined by plasma flow which is evidence that dust motion is predominantly due to drag force in quasineutral plasmas.

After x, y, z coordinates were found for each pair of dots, the three components of the velocity corresponding to two consecutive dots were given by their spatial separation divided by the frame-to-frame time, $U_x = \delta x/t_0, U_y = \delta y/t_0, U_z =$

$\delta z/t_0$. Average dust acceleration in three directions are obtained in the same way for two consecutive velocities divided by the frame-to-frame time: $a_x = \delta U_x/t_0, a_y = \delta U_y/t_0, a_z = \delta U_z/t_0$.

Dust accelerations were found to be hundreds to thousands times the gravitational acceleration in the radial, the azimuthal and the axial directions in cylindrical geometry, indicating that all of the three components of the plasma flow are substantial. Our measurements showed that dust velocities reached between 1 to 20 m/s due to plasma acceleration. The plasma acceleration force is about 100 to 1000 times the gravitational force. Therefore, gravitational acceleration of dust can be neglected in our experiment.

The shape of the dust conglomerates that we detected was irregular. However, for the sake of simplicity we approximated dust by spheres. Dust radius was measured from the images as follows. Dust emission in an image was fitted with a gaussian function in both 'a' and 'b' views, as shown in Fig. 3. Since an image is made up of pixels with different brightness the size corresponds to the full-width-half-maximum of a gaussian fit to the dust image. The image dust sizes are found to be comparable for different views and directions. The image size of the dust (d_e) is therefore selected to be the image dust size in the horizontal direction of the view 'a' for each dot. The 'real' dust radius (r_d) has been found based on its image size and the detection optics [15]. That is, $r_d = (\sqrt{d_e^2 - d_s^2})/(2M)$, where $d_s = 2.44(1+M)f^{\#}\lambda$ is the diffraction-limited spot diameter for the camera lens with $f^{\#}$ (= 4 for our experiment), and M is the magnification of the camera system, *i.e.* the ratio between the linear size of the image to that of the object. The CCD detector had a pixel size of 6.7 μm $\times$ 6.7 μm. The 10-nm-wide pass-band filter put in front of the optics had a center wavelength of $\lambda = 561$ nm. $M = 0.1$ for the experiment. The detected particles which were conglomerates of the dust powder were found to have a radius in the range of 100 to 200 μm. Therefore, individual dust particle radius is about 10 to 30 times the screening length $\lambda_D \simeq 5\mu$m, $(1/{\lambda_D}^2 = 1/{\lambda_{Di}}^2 + 1/{\lambda_{De}}^2$, where $\lambda_{Di,De}$ are the ion and electron Debye lengths, respectively) of the plasmas with $\simeq 10^{19}$ m^{-3} densities and ~ 10 eV temperatures.

The recorded dust traces for some dust particles were elongated along the plasma flow direction. A projection of the dust trajectory on the imaging plane is shown in Fig. 4. The arrows in the figure indicate just the inclination of these traces (not the flow direction) at successive moments in time with the horizontal. It can be seen that over a distance of a few millimeters the angle changes indicating different flow orientation. The size of the dust particle is smaller at a later time due to its movement out of the viewing region.

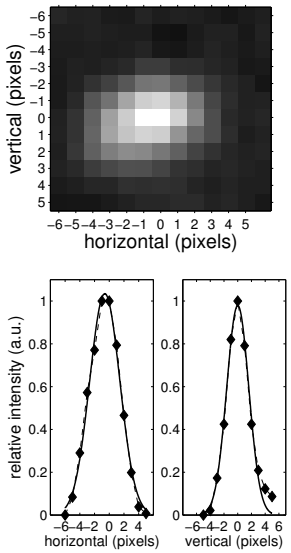

Fig. 3 – Gaussian fit for light emission of a dust particle captured by the CCD and visible pixels of the camera.

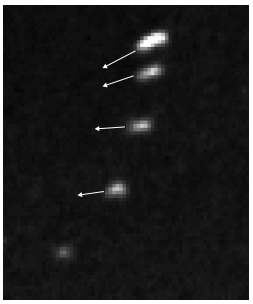

Fig. 4 – Dust particle captured by the CCD at successive times: the inclination of the dust trace with the horizontal is modified in time.

3. PLASMA DRAG FORCE ON DUST

Forces on moving dust particles in plasmas have been discussed extensively [1, 2, 5, 16–22]. The generic form of dust acceleration is the Newton's second law of motion in this context. We may exclude several forces: gravity (too small based on experimental data), neutral gas drag and thermophoretic force due to neutral particles (too small for gas density of a few mTorr), $\mathbf{U}_d \times \mathbf{B}$, where $\mathbf{U}_d$ is the dust speed (too small due to both the dust size and weak magnetic field ≤ 0.1 T), radiation pressure (small compared with gravity). Other possible forces on a dust in a quasineutral

plasmas may include plasma-flow drag, electric force, plasma pressure-gradient drag due to both electrons and ions $[\nabla(n_i T_i + n_e T_e)]$. We neglect the plasma pressure-gradient drag for both the axial (z-direction) and azimuthal (x-direction), since the pressure equilibration time in both direction are expect to happen within tens of μs for these directions, and the dust velocities and accelerations are averaged over hundreds of μs. Therefore, the remaining forces are the electric force (proportional to the electric field $\mathbf{E}$) and plasma-flow drag ($\mathbf{F}_{pf}$). The dust acceleration ($\mathbf{a}$) is described by

$$\rho_d \frac{4\pi r_d^3}{3}\mathbf{a} = \mathbf{F}_{pf} + Q_d\mathbf{E} \tag{1}$$

for a spherical dust particle with a radius r_d, mass density ρ_d, and a total charge electric Q_d.

The plasma-flow drag $\mathbf{F}_{pf}$ has mainly two contributions from the drifting ions, one from the long-range Coulomb collisions and the other from direct impact. The plasma drag on a dust particle has been widely investigated for particles much smaller than the plasma Debye length λ_D, which is a necessary condition for the applicability of the orbital motion limited theory (OML) [23]. The orbital component of the drag force has a contribution comparable with the direct impact force and is sensitive to the Coulomb logarithm given by the ratio of the plasma screening length to the ion impact parameter at 90^o [5]. This situation is typical for low ionized gases laden with microparticles such as those encountered in plasma processing reactors and in some particular cases for fusion reactors, when submicron particles are at the edge of the plasma. In this later case the particles can also be highly irregular in shape with a size spanning a few orders in magnitude, from hundreds of nanometers to fractions of millimeters. In our experiment the detected dust particles are in the range of 100 to 200 μm in radius, which is at least an order of magnitude larger than λ_D.

Since for our plasma conditions the argument of the Coulomb logarithm is $\simeq 1$ we conclude that momentum transfer through Coulomb collisions is negligible compared to the direct impact force of ions [16, 17]. Let's consider the dust particle surrounded by a thin sheath s_d of the order of a few screening lengths $\lambda_D < s_d \ll r_d$. Then the ions entering the sheath are further absorbed on the dust surface and contribute to the plasma drag force, while those passing by at a grazing distance are not perturbed in their trajectories. The drag exerted by the ion flow is similar to that of a flowing hot gas entraining dust. This scenario is only an approximation of the real situation, as the dust charge does not come into play. The force is given by [21, 22]

$$\mathbf{F}_{col} = \frac{16}{3}\sqrt{\pi} r_d^2 n_i k_B T_i \mathbf{w}\left(1 + \frac{9\pi}{64}\mathbf{w}^2\right)^{1/2}. \tag{2}$$

where $\mathbf{w} \equiv \mathbf{U_P}/\sqrt{2k_B T_i/m_i}$ is the plasma flow velocity $\mathbf{U_P}$ normalized to ion

thermal velocity, k_B is the Boltzmann constant, T_i the ion temperature, m_i the ion mass, and n_i the ion density. The dust velocity in $\mathbf{w}$ has been neglected since it is a few orders of magnitude less than the plasma flow. In air, a microparticle tracks flow with high fidelity and eventually its terminal speed is that the flow, however, in plasma flow dust velocity can be quite small compared with that of the flow.

For subsonic plasma flow ($\mathbf{w} < 1$), Eq. (2) can be approximated by a more convenient and simplified formula:

$$\mathbf{F}_{pf} = 2\pi r_d^2 n_i k_B T_i \xi \mathbf{w}. \tag{3}$$

where the coefficient $\xi = 1.1 \sim 1.6$ depends on the different models for the ion-dust surface interaction [21, 22].

To get more insight into the effect of the dust potential on ion collection we make a comparison with the ion drag force given by the OML theory [23]. The formula for the ion drag is the well-known expression for direct collisions obtained by integrating the momentum-transfer cross section over a Maxwell-Boltzmann distribution, which includes the ion flow [19, 20]:

$$\mathbf{F}_{col\ (OML)} = \sqrt{\pi} r_d^2 n_i k_B T_i \Bigg\{ \mathbf{w} \left(2 + \frac{1}{\mathbf{w}^2} + \frac{2\chi}{\mathbf{w}^2} \right) \exp\left(-\mathbf{w}^2\right) + \left[2\left(\mathbf{w}^2 + 1 - \frac{1}{4\mathbf{w}^2} \right) - \left(\frac{1}{\mathbf{w}^2} - 2 \right) \chi \right] \sqrt{\pi} \mathrm{erf}(\mathbf{w}) \Bigg\}, \tag{4}$$

where $\chi = -eV_d/k_B T_i$, and V_d is the dust potential. Rather than obtaining the dust potential in the usual manner from the cancelation of ion and electron currents at the dust surface in the OML framework, we base our reasoning on the conclusions of the sheath-limited theory. We suppose that ions conserve their orbital momentum in the presheath and as they approach the dust they are accelerated by the potential drop $eV_d \approx -1/2(k_B T_i + k_B T_e)$ at the sheath-presheath interface, as suggested in [20]. It is in the presheath which extends into the plasma where ions feel the potential of the dust. The ions in the presheath having a directed motion towards the dust grain and an impact parameter within $[r_d, r_d\sqrt{1 + k_B(T_i + T_e)/m_i \mathbf{U_P}^2}]$, will have their trajectories bent by the influence of this potential and eventually will end up on the dust surface after crossing the thin sheath. In Eq. (4) the sheath width s_d has been neglected and r_d has been taken instead of $r_d + s_d$. It should be reminded here that the OML theory is only valid when $\lambda_D \ll r_d$. Our present approach is presented here rather as an additional tool for estimating the plasma drag force and accounting for the attractive potential near the dust particle.

For plasma charged dust particles, the electric force is particularly important in the overall dust dynamics, especially in regions where electric fields are present. In our experiment the electric force can only come from inductive electric field for the x- and z-directions. The dust acceleration due to the electric force is plotted with

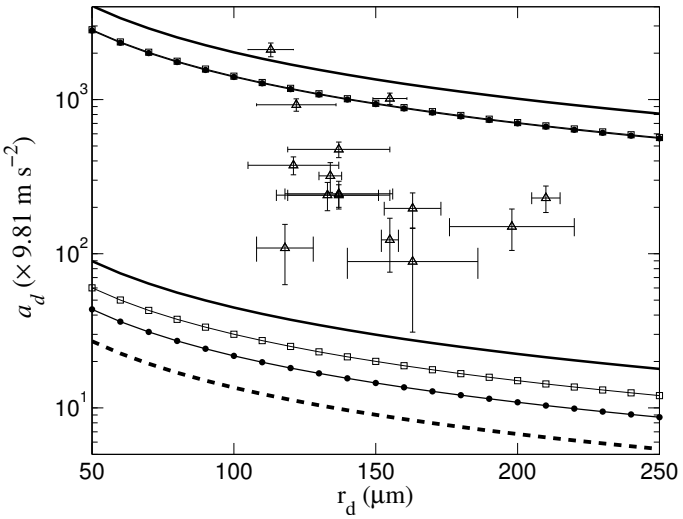

Fig. 5 – Measured dust acceleration with error bars and plasma drag models; the curves '..', '□', '-' are solutions of Eqs (2-4), respectively, while the curve '- -'is given by the electric force.

dashed line against experimental data in Fig. 5. It is given by $Q_d\mathbf{E}/m_d$ in Eq. (1), assuming an inductive electric field of $E \simeq 10^2$ V/m, and Q_d corresponds to a field-emission limited charge (using a theoretical upper limit $E_d = 10^8$ V/m) on a perfectly round dust particle for a given radius. The acceleration by electric force can be put in the following form: $a_{el} = 3\varepsilon_0 E_d E/r_d\rho_d$. The plasma-flow drag force is also plotted in Fig. 5: the solutions of equations 2, 3 and 4 are shown with dotted, square and continuous lines, respectively. Two sets of plasma parameters have been chosen: an upper limit using a plasma flow at Mach 0.6, $n_i = 4.0 \times 10^{19}$ m^{-3}, and $T_i = 15$ eV, and a lower limit corresponding to a small Mach number of 0.2, $n_i = 1.0 \times 10^{19}$ m^{-3}, and $T_i = 4$ eV. The parameter ξ of Eq. 3 becomes 1.6 and 1.1 for the two above sets. Experimental data matches fairly well the theoretical predictions from the plasma-flow drag model. One main conclusion is that the observed dust acceleration is predominantly due to plasma flow, as electrostatic acceleration is at least one order of magnitude lower. The accelerations given by Eqs. (2) and (3) converge at the higher values of plasma parameters. Dust acceleration given by Eq. (4) is in general higher then in the previous cases and it appears to be a better fit for the experimental data. This demonstrates the importance of the dust charge in evaluating ion drag and the necessity to include it in a rigorous approach. Of course, the model is for steady state plasma and does not account for non-uniformities in the flow such as variations in the density and temperature. These phenomena take place at a sub-millisecond timescale and can definitely affect dust acceleration. Also the dust size is only an

approximation obtained from the parameters of the optical system; the exact size may be slightly different.

4. CONCLUSIONS

In summary, we have measured the acceleration of large dust particles dragged by rotating quasineutral plasma flows with density $\simeq 10^{19}$ m^{-3} and temperature of $\simeq 10$ eV. Plasma-induced dust fluorescence, brighter than background plasma light at certain wavelengths, enabled the dual-camera imaging technique for dust tracking. Quantitative comparison of the dust acceleration with predictions of a simple model shows that plasma-flow drag is the primary force that determines the dust motion.

Acknowledgements. The author acknowledges partial support from the Ministry of Education under program LAPLAS 2013, within the PNCDI2 program.

REFERENCES

1. P. K. Shukla and B. Eliasson, Rev. Modern Phys. **81**, 25 (2009).
2. P. K. Shukla and A. A. Mamun, *Introduction to Dusty Plasmas* (IoP Publishing) (2002).
3. H. Thomas, G. E. Morfill, V. Demmel, J. Goree, B. Feuerbacher, D. M. and Möhlmann, Phys. Rev. Lett, **73**, 652 (1994).
4. J. H. Chu and I. Lin, Phys. Rev. Lett. **72**, 4009 (1994).
5. S. A. Khrapak, A.V. Ivlev, G. E. Morfill and H. M. Thomas, Phys. Rev. **E 66**, 046414 (2002).
6. R. L. Merlino and J. A. Goree, Phys. Today, **57**,32 (2004).
7. V. E. Fortov, A. G. Khrapak, V. I. Molotkov, and O. F. Petrov, Phys. Uspekhi, **47**, 447 (2004).
8. E. Thomas and J. Williams, Phys. Rev. Lett., **95**, 055001 (2005).
9. Z. Wang, C. M. Ticos and G. A. Wurden, Phys. Plasmas, **14**, 103701 (2007).
10. C. M. Ticos, Z. Wang, G. A. Wurden, J. L. Kline, D. S. Montgomery, L. A. Dorf and P. K. Shukla, Phys. Rev. Lett., **100** 155302 (2008).
11. Z. Wang, J. Si, W. Liu, and H. Li, Phys. Plasmas **15**, 102109 (2008).
12. http://www.luminescers.com/l-212.html; Beaver Luminescers, Two Newton Place, Suite 200, Newton, Massachusetts USA 02458.
13. C. M. Ticos, Z. Wang, L. A. Dorf, and G. A. Wurden, Rev. Sci. Instrum., **77**, 10E304 (2006).
14. J. Si and Z. Wang, Rev. Sci. Instrum., **77**, 10E311 (2006).
15. R. J. Adrian, Appl. Opt., **23**, 1690 (1984).
16. Z. Wang, C. M. Ticos, L. A. Dorf, and G. A. Wurden, IEEE Trans. Plasma Sci., **34**, 242 (2006).
17. C. M. Ticos, Z. Wang, G. L. Delzanno, and G. M. Lapenta, Phys. Plasma, **13**, 103501 (2006).
18. M. S. Barnes, J. H. Keller, J. C. Forster, J. A. O'Neill, and D. K. Coultas, Phys. Rev. Lett., **68**, 313 (1992).
19. A. A. Uglov and A. G. Gnedovets, Plasma Chem. Plasma Process., **11**, 2511991 (1991).
20. I. H. Hutchinson, Plasma Phys. Control. Fusion **48**, 185 (2006).
21. M. J. Barnes, I. P. Williams, and A. S. Asebiomo, Mon. Not. R. Astron. Soc. **130**, 63 (1965).
22. B. T. Draine and E. E. Salpeter, Astrophys. J. **231**, 77 (1979).
23. J. E. Allen, B. M. Annaratone, U. de Angelis, J. of Plasma Phys. **63**, 299 (2000).